J Solid State Electrochem (2010) 14:109–114
DOI 10.1007/s10008-009-0791-8

ORIGINAL PAPER

The effect of oxygen pressures on the electrochemical profile of lithium/oxygen battery

Xin-hui Yang · Yong-yao Xia

Received: 05 December 2008 / Revised: 11 January 2009 / Accepted: 18 January 2009 / Published online: 12 February 2009

Abstract The influences of oxygen pressure on the performance of a lithium/oxygen battery using non-aqueous electrolyte were investigated in this paper. Oxygen pressures were adjusted from 1 to 10 atm. It was found that, at all examined discharge rates from 0.1 to 1.0 mA cm^{-2}, the discharge capacity increased with the increasing of oxygen pressure, especially at a high discharge rate. The morphology of the discharge product was found to relate to discharge rate and oxygen pressure by scanning electron microscopy observation.

Keywords Li/air battery · Li/oxygen battery · Oxygen pressure

Introduction

Metal/air batteries are practically attractive because they offer potentially high energy densities. The air cathode active material, oxygen, is not stored internal to the cell/battery system. Oxygen from the environment is reduced at a catalytic air electrode surface forming either an oxide or peroxide ion that then reacts with cationic species in the electrolyte. The metal/air batteries have been developed based on different materials including Fe, Zn, Al, Mg, Ca, and Li. The characteristics of some metal/air battery couples are shown in Table 1. It shows that the lithium/air battery is the most promising because it has the highest theoretical specific energy of 11,140 Wh kg^{-1}. This energy density is significantly higher than that of a methanol/air fuel cell, which is 6,098 Wh kg^{-1}. Therefore, the energy density of lithium/air battery may be the limit of electrochemical power sources.

Lithium/air battery was first reported by Abraham and Jiang [1]. The battery overcomes the lithium corrosion in aqueous electrolyte by employing organic polymer electrolyte. The battery was shown to have an open-circuit potential close to 3 V, with an operating voltage between 2.0 and 2.8 V. The air electrode was composed of carbon black and cobalt phthalocyanine as catalyst. The overall cell reaction during discharge is $2Li\ (s)+O_2\ (g)\rightarrow Li_2O_2\ (s)$. In addition to this reaction, Read et al. regarded $2Li\ (s)+1/2O_2\ (g)\rightarrow Li_2O\ (s)$ as another reaction occurs in discharge process [2]. Recently, P. G. Bruce found that the electrochemical reaction $2Li^+ + 2e^- + O_2 \longleftrightarrow Li_2O_2$ was reversible and that charge/discharge cycling can be sustained over 10 s of cycles. This provides important evidences to support the feasibility of rechargeable lithium air batteries [3, 4].

The lithium/air organic electrolyte battery differs from the aqueous metal/air batteries in that the oxygen reaction product is insoluble in the organic electrolytes. Li_2O_2 and Li_2O are formed at or near the sites where peroxide ions, O_2^{2-}, or oxide ions, O^{2-}, are generated. Discharge is ceased by the choke of deposit to the air electrode. Read et al. have fruitful results on the influences of air cathode formulation and electrolyte composition to the discharge capacity and rate capability [5, 6]. They concluded that electrolyte formulation has the largest influence on cell performance and presumably on the nature of the deposit formed during discharge. The ratio of Li_2O_2 to Li_2O deposited is a function of electrolyte formulation. However, the kinetic mechanism of the reaction in air electrode is under discussion. Anode reaction takes place not only in the gas–solid–liquid three-phase interface

X.-h. Yang · Y.-y. Xia (✉)
Department of Chemistry and Shanghai Key Laboratory of Molecular Catalysis and Innovative Materials, Fudan University, Shanghai 200433, China
e-mail: yyxia@fudan.edu.cn

Table 1 Properties of metal/air batteries

Metal/air battery	Calculated OCV/V	Theoretical specific energy/Wh kg^{-1}	
		Including oxygen	Excluding oxygen
Li/O_2	2.91	5,200	11,140
Na/O_2	1.94	1,677	2,260
Ca/O_2	3.12	2,990	4,180
Mg/O_2	2.93	2,789	6,462
Zn/O_2	1.65	1,090	1,350

but also in the bulk electrolyte for the battery still works when air electrode is immerged in electrolyte. Solubility of electrolyte to oxygen is important when the reaction occurs in bulk-electrolyte-involved long-distance diffusion. On the other hand, oxygen partial pressure may be critical in the process of the three-phase reaction. However, previous research has neglected to consider the influence of oxygen pressure on the performance of lithium/air battery.

In this study, the influences of oxygen pressure on the discharge capacity of a lithium/air battery using non-aqueous electrolyte were investigated by discharge tests, electrochemical impedance spectroscopy, and scanning electron microscopy (SEM). The potential causes for the improved rate capability at high oxygen pressure will also be discussed.

Experimental

Preparation of air electrode

Carbon air cathodes were prepared by mixing a 20-wt.% emulsion of polytetrafluoroethylene (PTFE) with Super P carbon black (CB) manufactured by M.M.M. Carbon Belgium and manganite as catalyst. Manganite was synthesized by the method described in [7]. In a typical procedure, a solution of 5.89 g of $KMnO_4$ in 200 mL of deionized water was slowly added to a stirred solution of 2.0 g sucrose, 4.40 g of $MnSO_4{\cdot}H_2O$, 30 mL of water, and 3.0 mL of concentrated HNO_3. The resultant solution was then refluxed at 100°C under constant stirring for 6 h. After hot filtration, the brown solid product was heavily washed with deionized water and air dried. The air electrode was fabricated by compressing a mixture of carbon black, manganite, and binder PTFE in a weight ratio of CB–manganite–PTFE=75:15:10 onto an aluminum grid at 10 MPa. The electrodes were then punched in the form of disks typically with a diameter of 12 mm and then dried at 120°C for 12 h.

Coin cell construction and testing

The cell assembly was operated in a glovebox filled with pure argon. The cell has a 1-mm-thick Li foil as negative electrode and an air electrode as a positive electrode. These two electrodes are separated by a separator dipping with 1 M $LiClO_4$/propylene carbon (PC) electrolyte. This Li/separator/air electrode product was then sealed into 2016-type coin cell. To allow oxygen to diffuse into the electrode, a 4-mm-diameter opening was made on the cape side of the coin cell.

The cell was enclosed in a stainless steel can, where oxygen pressure was adjusted from 1 to 10 atm. As all of the experiments were measured in oxygen gas, lithium air battery is called lithium oxygen battery as well. Molecular sieve was placed in the can to prevent moisture. There is at least a 2-h rest for the cells before every test. Electrochemical measurements including discharge and polarization tests were conducted with a Solartron Instrument Model 1287 electrochemical interface controlled by a computer. This same instrument was then connected to a Solartron 1255 frequency response analyzer to measure the impedance spectra. For most of the tests, frequency limits were between 10^6 and 0.01 Hz with ac oscillation of 5 mV. The SEM images were obtained on Philip XL30 operated at 25 kV.

Results and discussion

Discharge profile

Figure 1 shows the discharge behavior of the air electrode in 1 M $LiClO_4$/PC electrolyte at four different rates. During the discharge process, the cell was exposed in 1 atm of dry

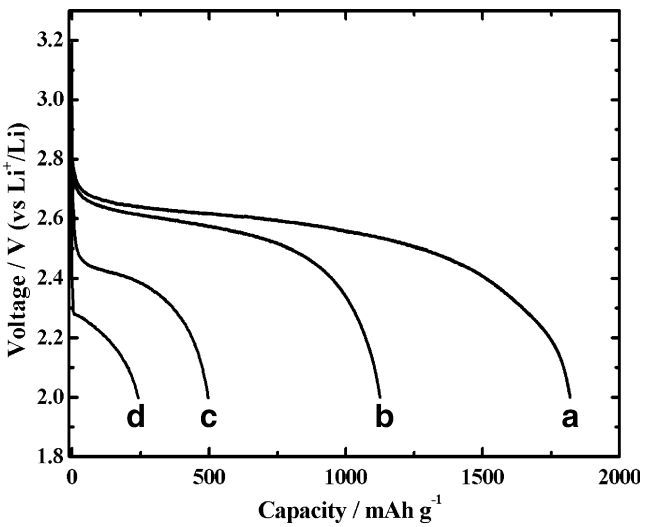

Fig. 1 Discharge curves of the lithium air cell in 1 atm of dry oxygen at different current densities at room temperature. (*a*) 0.1 mA cm^{-2}, (*b*) 0.2 mA cm^{-2}, (*c*) 0.5 mA cm^{-2}, (*d*) 1.0 mA cm^{-2}

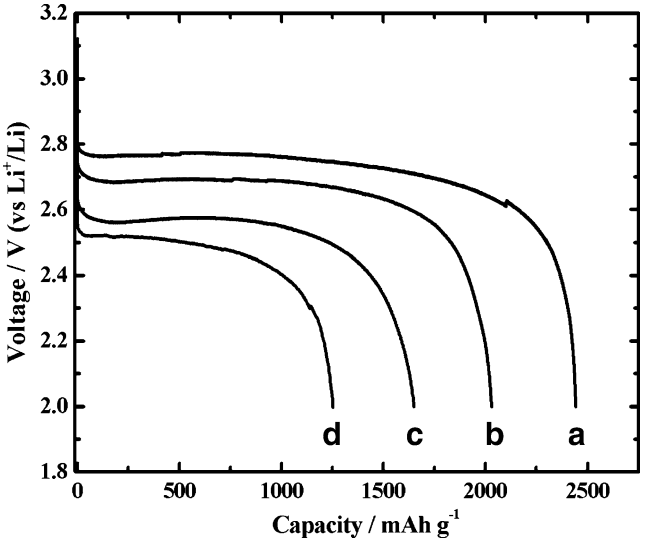

Fig. 2 Discharge curves of the lithium air cell in 10 atm of dry oxygen at different current densities at room temperature. (*a*) 0.1 mA cm^{-2}, (*b*) 0.2 mA cm^{-2}, (*c*) 0.5 mA cm^{-2}, (*d*) 1.0 mA cm^{-2}

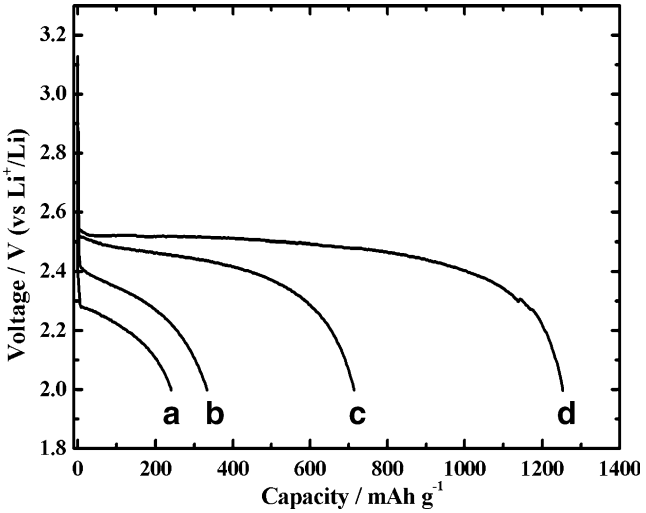

Fig. 4 Discharge curves of the lithium air cell at a fixed current density of 1.0 mA cm^{-2} in (*a*) 1 atm, (*b*) 3 atm, (*c*) 5 atm, and (*d*) 10 atm of oxygen

oxygen. The cell is in an open-circuit (OCV) of 3.10 V. The working voltage of the cell is ranged between 2.80 and 2.00 V, with an average of 2.60 V. According to the literatures [8], the capacity of lithium/air battery discharge reaction for every particular cell has been normalized to the weight of carbon in the air cathode. It is assumed that the products of the lithium/air battery discharge reaction deposit only onto carbon. The discharge capacity of 1,819 mAh g^{-1} is obtained at low current density of 0.1 mA cm^{-2}. Specific capacity decreases significantly and average voltage drops rapidly as discharge rate increases.

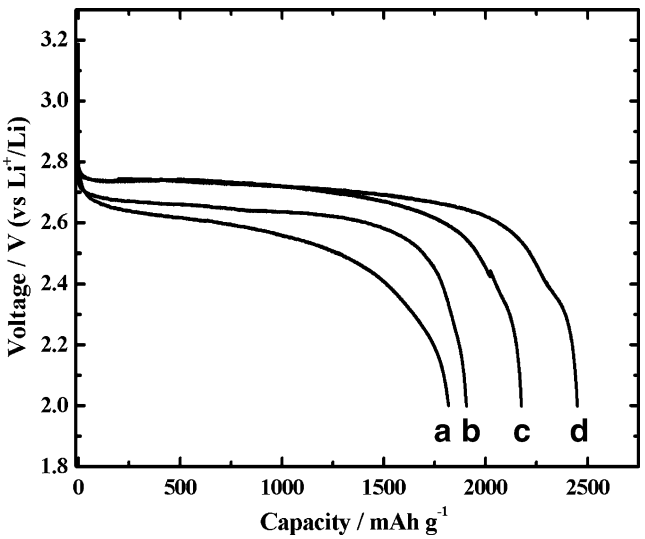

Fig. 3 Discharge curves of the lithium air cell at a fixed current density of 0.1 mA cm^{-2} in (*a*) 1 atm, (*b*) 3 atm, (*c*) 5 atm, and (*d*) 10 atm of oxygen

This situation is consistent with the results previously reported [9, 10]. The cell only delivers 15% capacity when the discharge rate increases from 0.1 to 1.0 mA cm^{-2}. It shows that the rate capacity of lithium/air battery is low in 1 atm oxygen. Similarly, Fig. 2 displays the discharge curves at different rates in 10 atm dry oxygen. The air electrode has a capacity of 1,252 mAh g^{-1} at a high discharge rate of 1.0 mA cm^{-2}, corresponding to 50% retention of that at 0.1 mA cm^{-2}. All findings suggest that the rate capacity improves in 10 atm oxygen.

Figure 3 shows the discharge curves of Li/air battery at 0.1 mA cm^{-2} under different oxygen pressures, varying from 1 to 10 atm. Average voltage increases from 2.60 to 2.72 V as the oxygen pressure increases from 1 to 10 atm. It delivers a specific capacity at 2,442 mAh g^{-1}, corresponding to 130% of that at 1 atm. Figure 4 displays the discharge capacity at high rate in different pressures of oxygen. There is a clear increasing trend of capacity for oxygen pressures increasing from 1 to 10 atm. The discharge capacity increases five times to 1,252 mAh g^{-1} in 10 atm compared to that in 1 atm. Table 2 summarizes the specific capacity of Li/air battery at different current

Table 2 Specific capacity of carbon in various pressures of oxygen

Oxygen pressure/atm	Specific capacity (mAh g^{-1}) at a specified rate (mA cm^{-2})			
	0.1	0.2	0.5	1.0
1	1,819	1,126	496	240
3	1,906	1,442	905	333
5	2,177	1,736	1,261	714
10	2,442	2,032	1,650	1,252

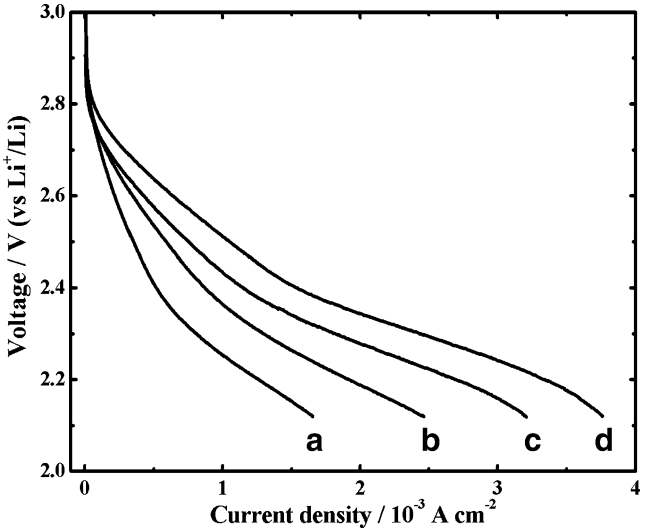

Fig. 5 Polarization curves for oxygen reduction with carbon black air electrode in (*a*) 1 atm, (*b*) 3 atm, (*c*) 5 atm, and (*d*) 10 atm of oxygen

rates under different oxygen pressures. It demonstrates that, with the same current rate, the Li/air battery has a larger capacity at a higher pressure, especially at a high current rate of 1.0 mA cm^{-2}.

The polarization curves for oxygen reduction measured under different oxygen pressures are shown in Fig. 5. The polarization curve measurements were run between 3.0 and 2.1 V (scan rate, 1 mV s^{-1}). Potentials were corrected for ohmic drop by the current-interrupter method. When the oxygen pressure is increasing, the potential of electrodes also increases. It agrees well with the results derived from the discharge curves.

Morphology of air electrode

Figure 6 displays SEM images of the airside of air electrodes under different discharge conditions and oxygen pressures. Individual particles of Super P carbon black are

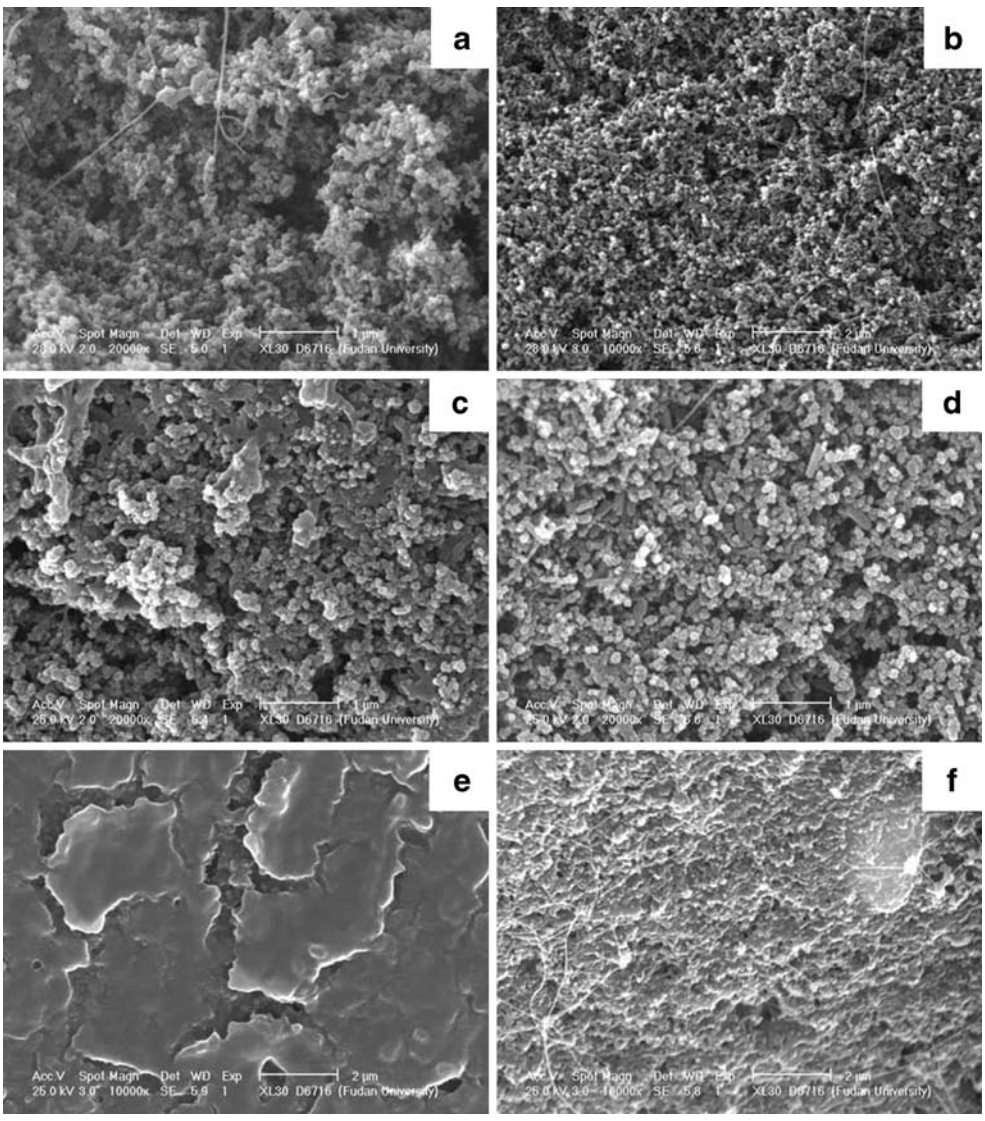

Fig. 6 SEM micrographs of the air side of air electrode **a**, **b** undischarged and discharged at **c** 0.1 mA cm^{-2} in 1 atm oxygen, **d** 0.1 mA cm^{-2} in 10 atm oxygen, **e** 1.0 mA cm^{-2} in 1 atm oxygen, and **f** 1.0 mA cm^{-2} in 10 atm oxygen. *Scale bar* of **a**, **c**, and **d** is 1 μm and that of **b**, **e**, and **f** is 2 μm

visible in the undischarged electrode with a primary particle size of about 50 nm. After a low discharge rate at 0.1 mA cm^{-2} in 1 atm oxygen, the electrode surface contains discharge products: particles with a diameter of 100 nm. These particles are bright in the image. A similar image was taken after discharge at 0.1 mA cm^{-2} in 10 atm oxygen. The deposition chokes the pores of the air electrode and determines the discharge process. After a high discharge rate at 1.0 mA cm^{-2} in 1 atm oxygen, the deposition formed a film adhering to the surface of electrode. This film prevents further reaction between Li^+ and oxygen; therefore, it results in a significant loss of specific capacity. In contrast, no obvious film is observed in the electrode surface after 1 mA cm^{-2} in 10 atm oxygen. The surface is much denser than that of low discharge rate. It is believed that some of the discharge products are formed in the inner pores of the electrode because no pore is left in the image. In another word, the different amount of discharge product causes the significant differences of capacity. For 1 mA cm^{-2} discharge rate, the capacity is 240 mAh g^{-1} in 1 atm oxygen, compared to a 1,252 mAh g^{-1} capacity in 10 atm oxygen.

Impedance properties

Figure 7 shows Nyquist plots for the battery including air electrode and lithium metal electrode at OCV at the beginning and at the end of discharge at different rates in 1 and 10 atm oxygen, respectively. These Nyquist plots present distorted semicircles. The further analysis of the impedance is based on the equivalent circuit shown in the inset of Fig. 7. The model includes external ohmic resistance, R_e, which is a combination of the uncompensated electrolyte resistance between the working and the counter electrode, an electronic resistance of the current collector, and any contact resistance that may exist between the external surface of the electrode and the electrolyte. The internal ohmic resistance, R_m, is a combination of the electrolyte resistance within the electrode, the electronic resistance of the electrode material, and the contact resistance between the electrode components. R_k is kinetic resistance. In addition, the double layer capacitance is distributed according to the difference in the magnitude of the time constant, between the ohmic and faradaic processes, and represented by C_{d1} and C_{d2}, respectively.

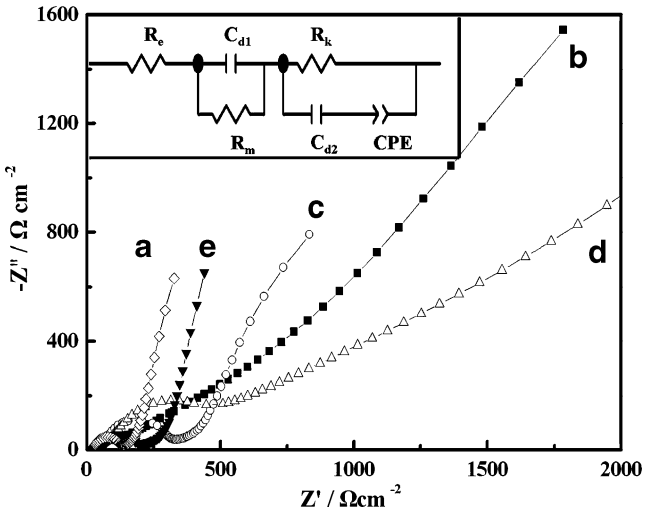

Fig. 7 Complex impedance plots of air battery at OCV (*a*) before discharge and after discharge at a current density of (*b*) 0.1 mA cm^{-2}, (*c*) 1 mA cm^{-2} in 1 atm of oxygen, (*d*) 0.1 mA cm^{-2}, and (*e*) 1 mA cm^{-2} in 10 atm of oxygen. The points are simulated data obtained by using the equivalent-circuit model shown as *inset*. *Inset*, equivalent circuit employed to stimulate the impedance diagrams obtained under OCP conditions. R_e is external ohmic resistance, R_m is mass transport resistance, R_k is kinetic resistance, CPE is constant phase element, and C_{d1} and C_{d2} are double-layer capacitances distributed between the ohmic and faradaic processes, respectively

Table 3 Equivalent circuit parameters of electrodes (a) before discharge and after discharge at current density of (b) 0.1 mA cm^{-2}, (c) 1 mA cm^{-2} in 1 atm of oxygen, (d) 0.1 mA cm^{-2}, and (e) 1 mA cm^{-2} in 10 atm of oxygen

Electrodes	R_e/Ω cm^{-2}	R_m/Ω cm^{-2}	R_k/Ω cm^{-2}	C_{d1}/ μF cm^{-2}	C_{d2}/ μF cm^{-2}
a	10.39	76.8	5,400	294	1.76
b	24.01	169	9,061	178	0.73
c	13.64	187.5	2,859	282	1.50
d	21.66	197.8	12,038	128	0.41
e	26.66	91.7	7,058	227	0.94

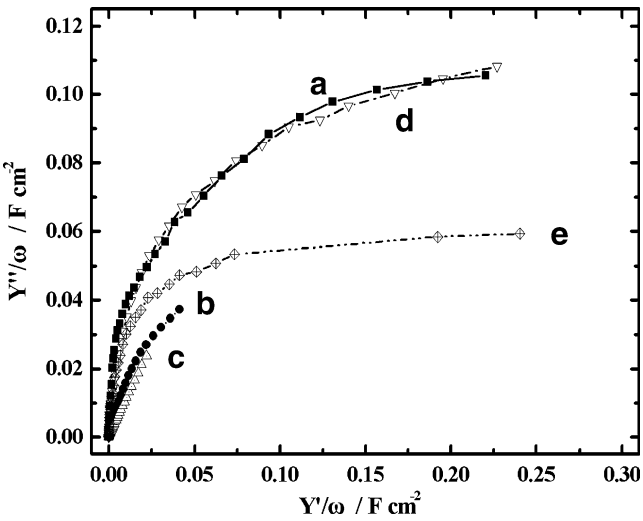

Fig. 8 Capacitance plots for the air electrodes which are (*a*) undischarged, discharged at (*b*) 0.1 mA cm^{-2}, (*c*) 1.0 mA cm^{-2} in 1 atm of oxygen, (*d*) 0.1 mA cm^{-2}, and (*e*) 1.0 mA cm^{-2} in 10 atm of oxygen. The impedance data were collected at open-circuit potentials. The *y-axis* represents the frequency-dependent series capacitance of the air electrode, Y''/ω, where Y'' is the imaginary component of the admittance and ω is the angular frequency

A quantitative analysis was performed to estimate ohmic, kinetic, and mass transfer resistances and double-layer capacitance by fitting the impedance spectra with model. The values of the equivalent circuit components were obtained using the program of Zview.

The parameters obtained by analyzing the data in Fig. 7 are listed in Table 3. The external ohmic resistance of electrodes after discharge, R_e, was set as 20 Ω cm^{-2} approximatively. There is a negligible difference that could be ascribed to the experimental error. Due to the erosion of the lithium cathode after a long-time exposure to oxygen, R_e is much higher than the conventional air electrode. The R_e of electrodes after discharge increases two times more than that of before discharge. On the other hand, the kinetic resistance, R_k, greatly differs for the electrodes. Extremely high resistances are shown for the low conductivity of the reaction product. Electrode D which was post-discharged in 0.1 mA cm^{-2} in 10 atm oxygen has the highest R_k. The amount of reaction product is proportional to R_k, and the order of R_k for the four electrodes is consistent to the order of specific capacitance. In contrast, C_{d1} and C_{d2} are in reversed order of R_k. This will be further discussed below.

Figure 8 demonstrates the 'capacitance' plots for electrodes. This format shows the series capacitance, which is proportional to the electrochemically accessible surface area of the electrode [11, 12]. The capacitance was determined by extrapolating the semicircles to the imaginary axis. Figure 8 describes the capacitance variation of electrodes. The cells in Fig. 8 are pre-discharged, post-discharged at 0.1 and 1.0 mA cm^{-2} current in 1 atm oxygen, and post-discharged at 0.1 and 1.0 mA cm^{-2} in 10 atm oxygen, respectively. The capacitance increases with the decreasing of frequency, because more of the active area of the electrode is accessed when the frequency decreases. It shows an increasing capacitance in the order of 0.1 mA cm^{-2} post-discharged in 10 atm <0.1 mA cm^{-2} in 1 atm oxygen <1.0 mA cm^{-2} post-discharged in 10 atm oxygen <1.0 mA cm^{-2} post-discharged ≤ pre-discharged electrode. The result is the same as the order of C_{d1} and C_{d2} given above. For the electrode with 2 mg cm^{-2} carbon, a specific capacitance of 48 F g^{-1} carbon was obtained. The capacitance decreased to 7.5 F g^{-1} for the post-discharged in 0.1 mA cm^{-2} in 10 atm oxygen.

Previous researches proved that capacitance is related to the electrolyte-accessible surface of electrodes [13]. A reduction of the capacitance means a portion of surface has been filled with the discharge product. The capacitances of 1.0 mA cm^{-2} post-discharged in 1 atm electrode and pre-discharged electrode are very similar. This similarity indicates that little electrode surface has been utilized for the electrochemical reaction. Under the 1.0 mA cm^{-2} post-discharged electrode in 10 atm oxygen experiment setting, there is a 23 F g^{-1} decrease of capacitance compared to that of the capacitance in 1 atm. This decrease indicates that significantly more pores of the electrode have been filled by the discharge product in this experiment setting. The capacitance result is consistent with the SEM images and the discharge curves.

Conclusion

The results of the discharge curves, polarization curves, impedance spectra, and SEM images exhibit that oxygen pressure has considerable influence on the performance of lithium/air battery, especially under a high discharge rate. The specific capacity is exceptionally low under high discharge rate due to the formation of discharge product film on the air side of electrode. This film has low conductivity, therefore preventing oxygen diffusion and terminating the electrochemical reaction. Increasing the oxygen pressure appears to be helpful in preventing this film from forming. In high-pressure oxygen, the improvement of high rate performance is remarkable.

References

1. Abraham KM, Jiang Z (1996) J Electrochem Soc 143:1–5. doi:10.1149/1.1836378
2. Read J (2002) J Electrochem Soc 149:A1190–A1195. doi:10.1149/1.1498256
3. Ogasawara T, Debart A, Holzapfel M, Novak P, Bruce PG (2006) J Am Chem Soc 128:1390–1393. doi:10.1021/ja056811q
4. Debart A, Bao JL, Armstrong G, Bruce PG (2007) J Power Sources 174:1177–1182. doi:10.1016/j.jpowsour.2007.06.180
5. Read J (2006) J Electrochem Soc 153:A96–A100. doi:10.1149/1.2131827
6. Read J, Mutolo K, Ervin M, Behl W, Wolfenstine J, Driedger A, Foster D (2003) J Electrochem Soc 150:A1351–A1356 doi:10.1149/1.1606454
7. Crisostomo VMB, Ngala JK, Alia S, Dobley A, Morein C, Chen CH, Shen X (2007) S.L. suib. Chem Mater 19:1832–1839. doi:10.1021/cm062871z
8. Kuboki T, Okuyama T, Ohsaki T, Takami N (2005) J Power Sources 146:766–769. doi:10.1016/j.jpowsour.2005.03.082
9. Sandhu SS, Fellner JP, Brutchen GW (2007) J Power Sources 164:365–371. doi:10.1016/j.jpowsour.2006.09.099
10. Sandhu SS, Brutchen GW, Fellner JP (2007) J Power Sources 170:196–209. doi:10.1016/j.jpowsour.2007.04.006
11. Ahn S, Tatarchuk BJ (1995) J Electrochem Soc 142:4169–4175. doi:10.1149/1.2048480
12. Arai H, Muller S, Haas O (2000) J Electrochem Soc 147:3584–3591. doi:10.1149/1.1393943
13. Jia N, Martin RB, Qi Z, Lefebvre MC, Pickup PG (2001) Electrochim Acta 46:2863–2869. doi:10.1016/S0013-4686(01)00511-4